

The cross-correlation parameters of the infrasonic wave field on the ground

Ludwik Liszka

IRF Scientific Report 303

July 2012

ISSN 0284-1703

Institutet för rymdfysik

Swedish Institute of Space Physics

Umeå, Sweden

The cross-correlation parameters
of the infrasonic wave field
on the ground

Ludwik Liszka

IRF Scientific Report 303

July 2012

Institutet för rymdfysik
Swedish Institute of Space Physics

Umeå, Sweden

IRF Scientific Report 303
ISSN 0284-1703
ISBN 978-91-977255-9-0

Swedish Institute of Space Physics
Box 812
SE-981 28 Kiruna
SWEDEN
www.irf.se

The cross-correlation parameters of the infrasonic wave field on the ground

Ludwik Liszka
Swedish Institute of Space Physics
Teknikhuset
90187 Umea, Sweden

1. Introduction

At the end of the 1950's and the beginning of the 1960's, the foundations for satellite communication and the global positioning system were created through a worldwide study of the statistical properties of radio wave propagation. Numerous projects (e. g. Liszka, 1963) were aimed at the study of the statistical structure of the wave field at the receiving antenna. That information was necessary to allow appropriate design of the receiving systems, which would take into account the specific properties of the signal.

The physical foundations of long distance propagation of radio waves are similar to those of infrasound. The first discovery of long distance propagation of infrasound is dated to the eruption of Krakatoa, August 27, 1883 when the pressure pulse from the eruption was recorded in Europe after it travelled around the earth. When the long distance propagation of infrasound was re-discovered during the 1960's, the research was concentrated on cataclysmic events, like nuclear explosions in the megaton-class. The knowledge that even many commonly occurring human activities may generate infrasound, which may be recorded at large distances, first came during the 1970's (Liszka, 1974). For many years to come, the long distance propagation of infrasound was a low-priority research area. Only when the Comprehensive Test Ban Treaty (CTBT) was actualized during the 1990's, did infrasound propagation research become a relevant topic again. At present, the CTBT infrasound network uses classical microbarographic technique from the 1960's and data analysis uses contemporary signal processing techniques developed for seismology. However, the propagation of infrasound in the atmosphere may be more similar to radio wave propagation in the ionosphere (Davies, 1972) than the propagation of seismic waves in the solid earth.

In order to properly address the problem of infrasonic detection one must carefully investigate the statistical properties of the infrasonic wave field on the ground and in particular of its anisometry. The statistical properties of the infrasound field on the ground vary differently in different directions, which is reflected in the fact that the cross-correlation in the wave field is direction dependent. These properties of infrasound wave field are of great importance in areas like signature recognition and spatial filtering.

2. Anisometry of the cross-correlation

The cross-correlation between microphones in an infrasonic array drops after a certain distance, even in a direction perpendicular to the propagation direction. This suggests that we are not observing plane waves.

In general, the cross-correlation varies both in the horizontal plane (x, y) and in time (t). The problem may be described by three ellipses: in the xt , yt and xy planes. When measuring the cross-correlation between two microphones in the x -direction, the cross-correlation drops

to a certain value at a distance x since the wave field also changes in time due to interaction with varying atmospheric structures. In general, in the xt -plane (see Fig. 1) we are considering Q as the maximum cross-correlation. The apparent velocity, V' , with which the wave pattern on the ground changes, will be:

$$V' = x'/t'$$

The true change velocity, V , will be instead:

$$V = x_m/t_m$$

Correlation ellipse in xt -plane

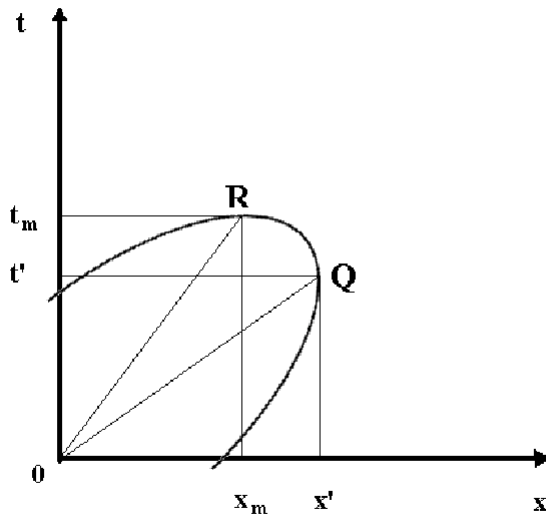


Fig. 1. Correlation ellipse in xt -plane

In practice, we have to consider all three correlation ellipses at the same time and to determine parameters of the 3-D correlation surface:

$$\rho = \rho(x, y, t).$$

It will be assumed that the surface may be approximated by the ellipsoid:

$$ax^2 + 2hxy + by^2 + 2fxt + 2gyt + ct^2 = D.$$

The ellipsoid parameters may be determined from a 3-microphone array when autocorrelations at all microphones and maximum cross-correlations between all three microphone pairs are determined. The numerical procedure, which has been used to describe the correlation pattern of radio waves on the ground, may be found in the literature (cf. e. g. Koster et al., 1965).

The correlation ellipse on the ground at a given time (in the xy -plane) will, in general, be rotated by an angle ψ (with the local North direction). For plane waves that angle will differ from the angle-of-arrival of the wave by 90 degrees.

The ellipsoid must be rotated along the t -axis by that angle in order to obtain useful ellipsoid parameters. Usually, the following parameters are used to describe the correlation pattern on the ground:

1. Axial ratio: $\sqrt{(b/a)}$,
where a is the size of the minor axis and b is the size of the major axis.
2. Size of the minor axis of the ellipse, calculated to the distance where the cross-correlation drops to $1/e$: $\sqrt{(\ln(1/e)/b * (\ln \rho_{ii}(x_1)))}$

where $\rho_{ii}(x_1)$ is the value of the autocorrelation function corresponding to one sampling period.

3. Eccentricity: $\sqrt{1 - (b/a)}$.

Both axes of the correlation ellipse, a and b , having a simple physical interpretation, will be used here. The minor axis is the correlation distance along the direction of propagation, while the major axis is the correlation distance along the wave front. The minor axis is related to the frequency content of the signal.

Examples of a few typical infrasonic signals presented in this study show temporal variations of:

1. Angle-of-arrival
2. Size of the minor axis
3. Size of the major axis

Also distributions of both axes of the correlation ellipse during an event may be of interest.

2.1. A close meteoroid entry

The example shows (Fig. 2) statistical properties of the infrasonic signal from a close meteoroid entry recorded at the Kiruna array. The meteoroid entry was localized to the mountains West of Kiruna (67.72N 17.51E), 123 kilometres from the Kiruna array.

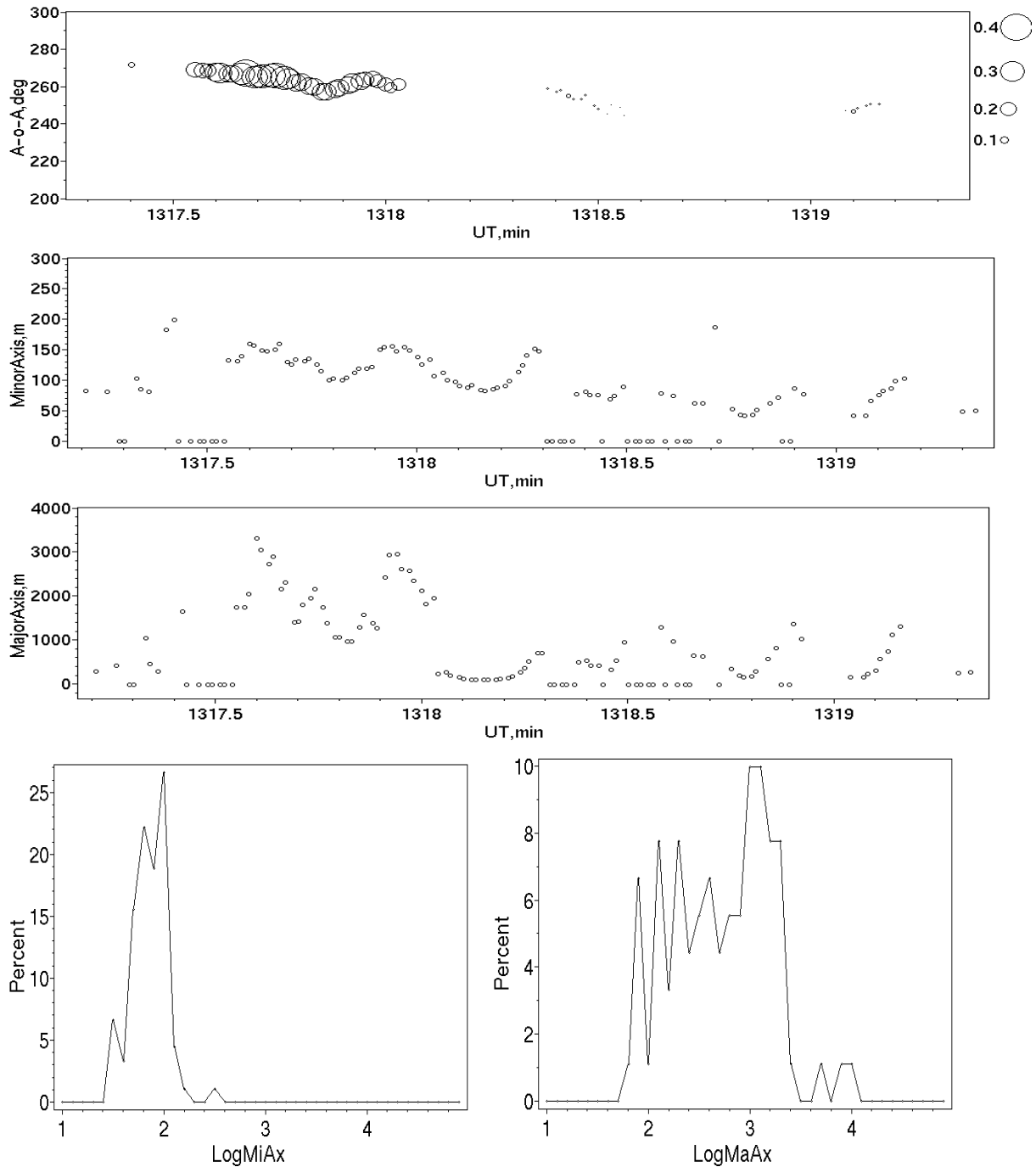


Fig. 2. Statistical properties of infrasonic signal from a close meteoroid entry on November 8, 2008, recorded at the Kiruna array, distance 123 km.

The **top graph** shows the angle-of-arrival of the signal as a function of time in minutes UT. The size of symbols is proportional to the product of cross-correlations between all three pairs of microphones. The **second graph** shows the size of the minor axis of correlation ellipse (in metres) as a function of time in minutes UT. The **third graph** shows the size of the major axis of correlation ellipse (in metres) as a function of time in minutes UT. The **left bottom graph** shows the probability distribution (in percent) of different sizes of the minor axis (logarithmic scale), while the **right bottom graph** shows the probability distribution (in percent) of different sizes of the major axis (logarithmic scale).

2.2. A distant meteoroid entry

The example shows (Fig. 3) statistical properties of the infrasonic signal from a distant meteoroid entry recorded at the Kiruna array. The meteoroid entry was localized to the North Sea, North of The Netherlands, 1744 kilometres from the Kiruna array.

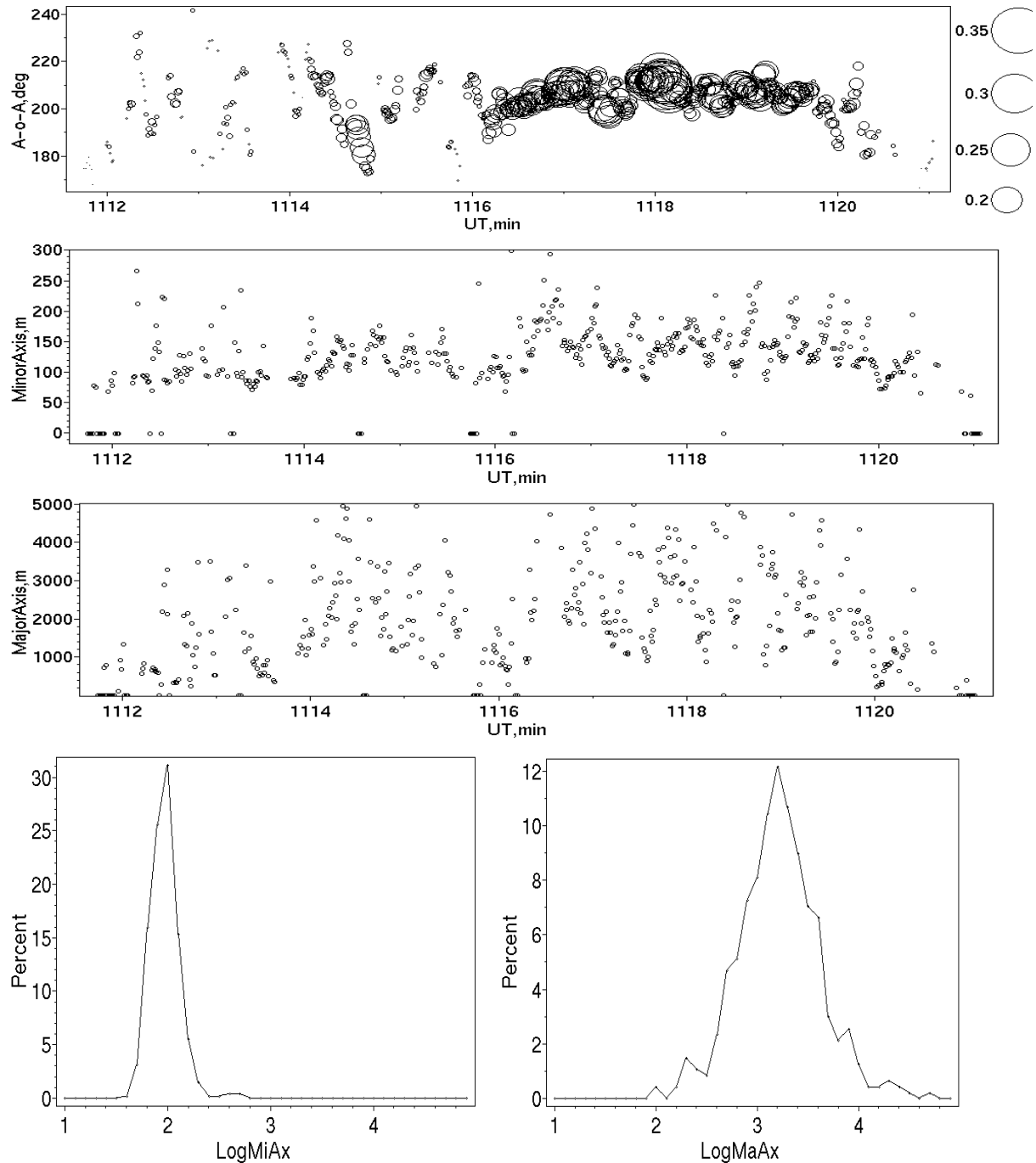


Fig. 3. Statistical properties of infrasonic signal from a distant meteoroid entry on November 8, 2008, recorded at the Kiruna array, distance 1744 km.

The **top graph** shows the angle-of-arrival of the signal as a function of time in minutes UT. The size of symbols is proportional to the product of cross-correlations between all three pairs of microphones. The **second graph** shows the size of the minor axis of correlation ellipse (in metres) as a function of time in minutes UT. The **third graph** shows the size of the major axis of correlation ellipse (in metres) as a function of time in minutes UT. The **left bottom graph** shows the probability distribution (in percent) of different sizes of the minor axis (logarithmic scale), while the **right bottom graph** shows the probability distribution (in percent) of different sizes of the major axis (logarithmic scale).

2.3. Small supersonic jets at distances 400-500 km

The infrasound from small supersonic jets (Fig. 4) was recorded at the Jämtön array in Northern Sweden on October 23, 1995. Three jets are flying towards the North with a supersonic speed along a trajectory at distances of 400-500 kilometres from the Kiruna array. The jets are separated in time by approximately 5 minutes.

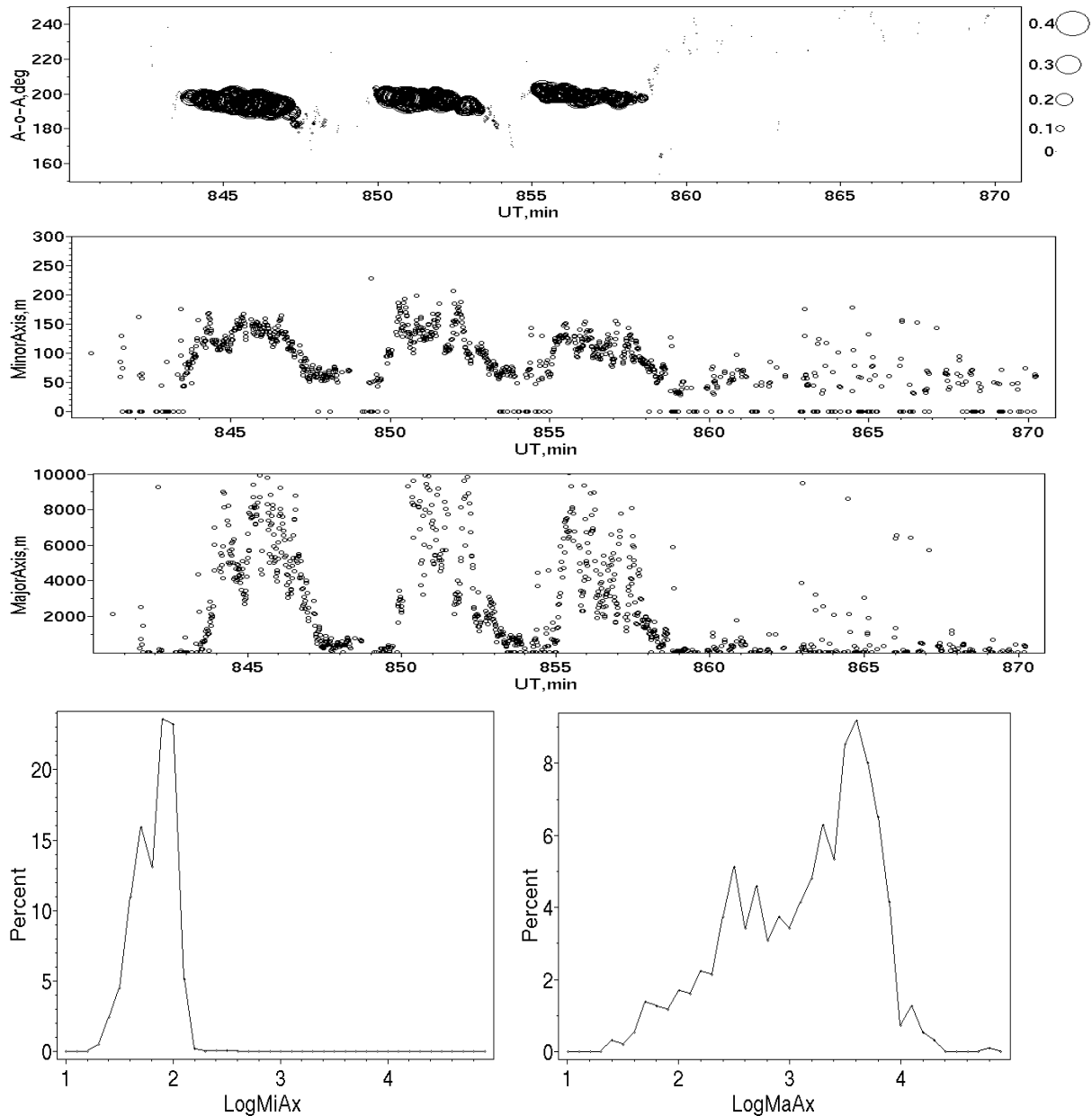


Fig. 4. The infrasound from small supersonic jets recorded at the Jämtön array October 23, 1995. The jets were flying with supersonic speed towards the North at distances of 400-500 km.

The **top graph** shows the angle-of-arrival of the signal as a function of time in minutes UT. The size of symbols is proportional to the product of cross-correlations between all three pairs of microphones. The **second graph** shows the size of the minor axis of correlation ellipse (in metres) as a function of time in minutes UT. The **third graph** shows the size of the major axis of correlation ellipse (in metres) as a function of time in minutes UT. The **left bottom graph** shows the probability distribution (in percent) of different sizes of the minor axis (logarithmic scale), while the **right bottom graph** shows the probability distribution (in percent) of different sizes of the major axis (logarithmic scale).

2.4. The large gas pipeline explosion on April 24, 1995, distance 1400 km

The explosion took place at Komi district, Russian Federation, at a distance of 1400 kilometres from the Kiruna array. The signal at 0 UT is the final part of the signal from a Concorde-flight.

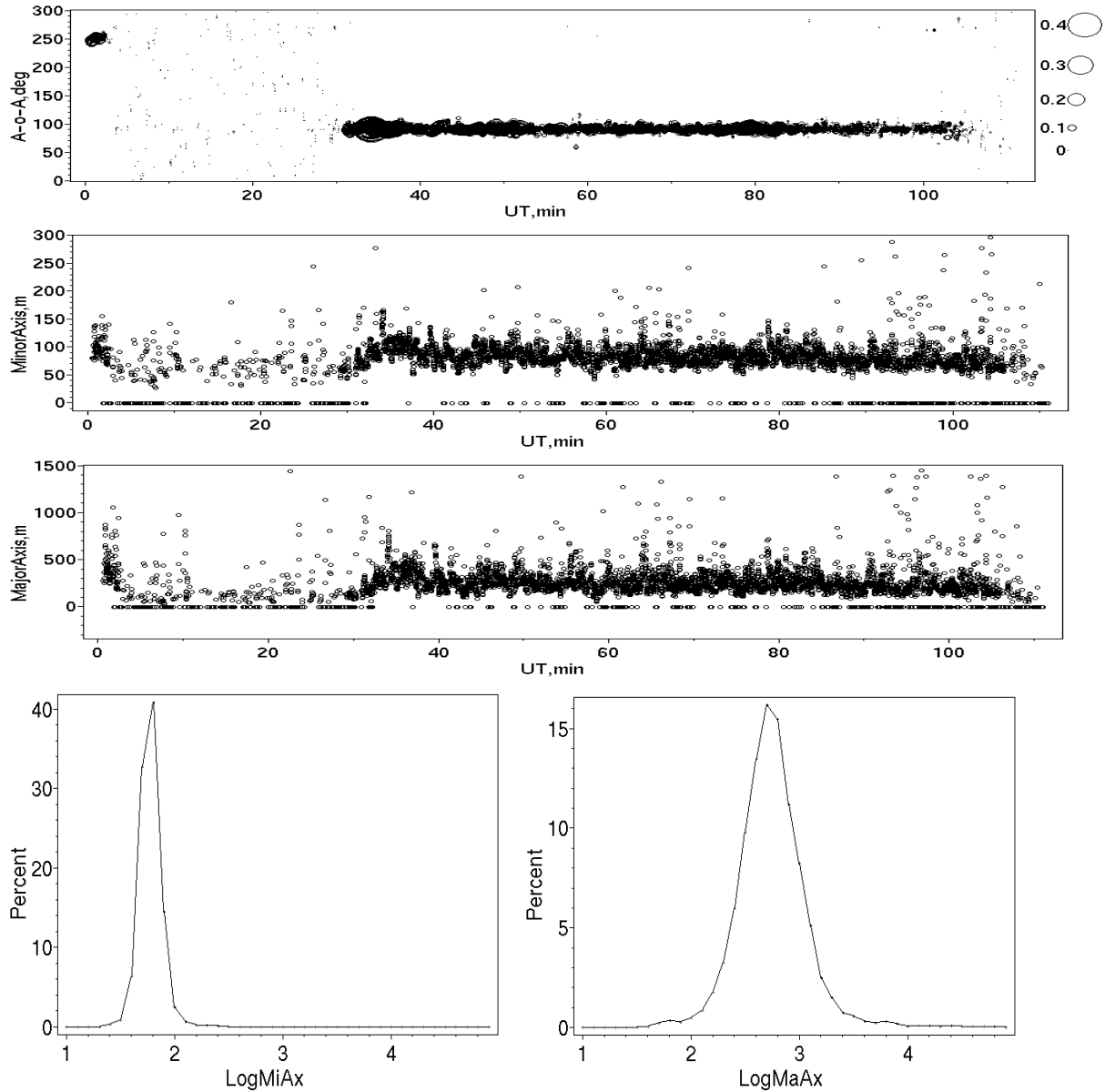


Fig. 5. The infrasound from a gas pipeline explosion recorded at the Jämtön array on April 24, 1995. The **top graph** shows the angle-of-arrival of the signal as a function of time in minutes UT. The size of symbols is proportional to the product of cross-correlations between all three pairs of microphones. The **second graph** shows the size of the minor axis of correlation ellipse (in metres) as a function of time in minutes UT. The **third graph** shows the size of the major axis of correlation ellipse (in metres) as a function of time in minutes UT. The **left bottom graph** shows the probability distribution (in percent) of different sizes of the minor axis (logarithmic scale), while the **right bottom graph** shows the probability distribution (in percent) of different sizes of the major axis (logarithmic scale).

2.5. A local thunderstorm passing by the microphone array - minimum distance 10 km

A small thunderstorm cell passes East of the Jämtön array during the evening of April 24, 1995. The closest distance to the array is approximately 10 kilometres.

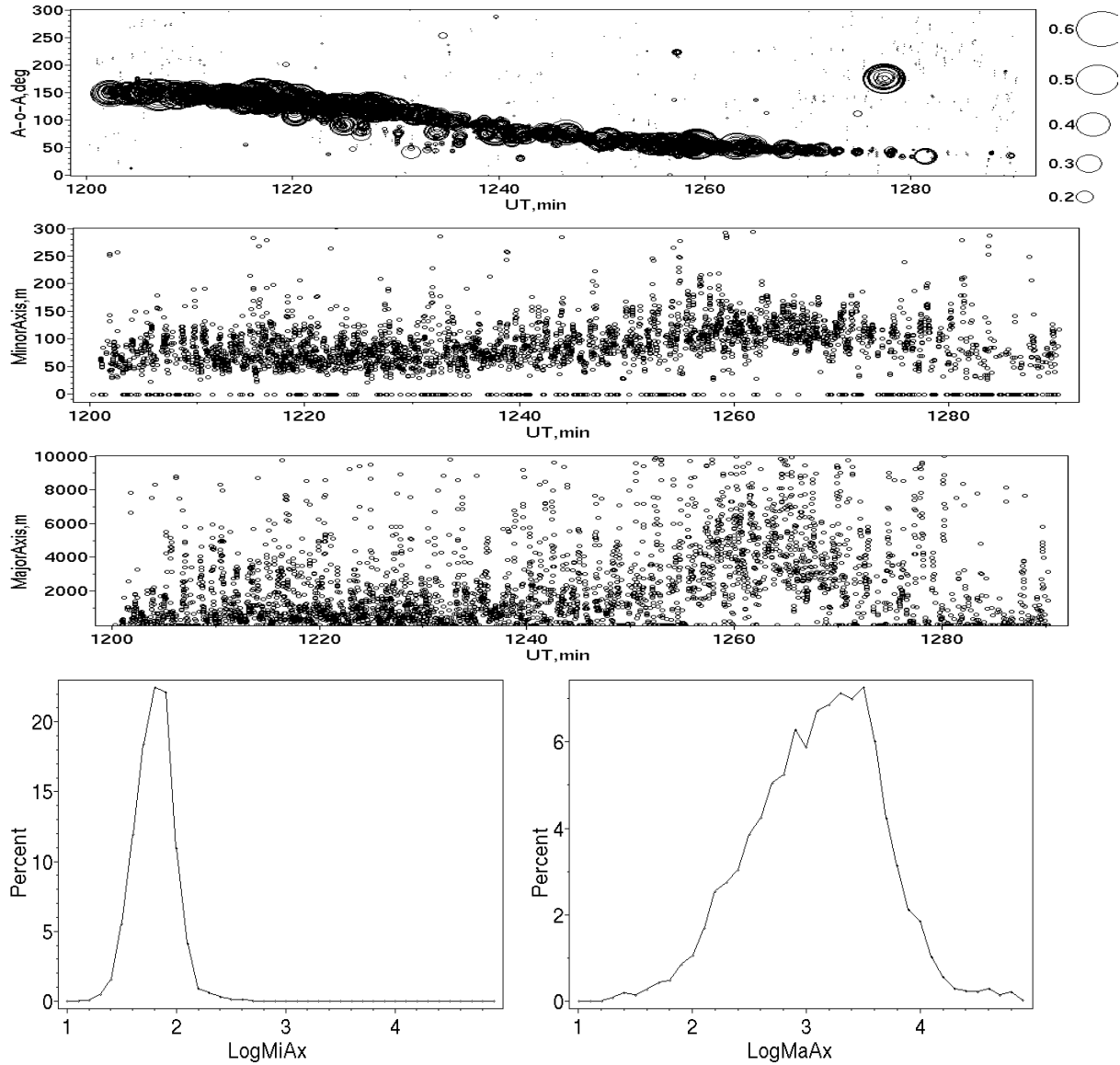


Fig. 6. The infrasonic from a small thunderstorm cell recorded at the Jämtön array on April 24, 1995. The thunderstorm passes East of the array at a closest distance of 10 km.

The **top graph** shows the angle-of-arrival of the signal as a function of time in minutes UT. The size of symbols is proportional to the product of cross-correlations between all three pairs of microphones. The **second graph** shows the size of the minor axis of correlation ellipse (in metres) as a function of time in minutes UT. The **third graph** shows the size of the major axis of correlation ellipse (in metres) as a function of time in minutes UT. The **left bottom graph** shows the probability distribution (in percent) of different sizes of the minor axis (logarithmic scale), while the **right bottom graph** shows the probability distribution (in percent) of different sizes of the major axis (logarithmic scale).

3. The anisometry of the cross-correlation on the ground and its consequences for signal detection

To measure the instantaneous intensity pattern on the ground would be very difficult and expensive. However, when the cross-correlation function over the ground is known, it is possible to simulate an intensity field, which would have an identical cross-correlation function (Wernik, private communication) to the one measured. Assuming a typical low frequency signal with an axial ratio of 5, a minor axis of the ellipse of the order of 100 metres, a $1/f$ noise spectrum and a direction-of-arrival of 60 degrees, the intensity field on the ground may be simulated. The result of a simulation for an area of 1024 x 1024 metres is shown in Fig. 7.

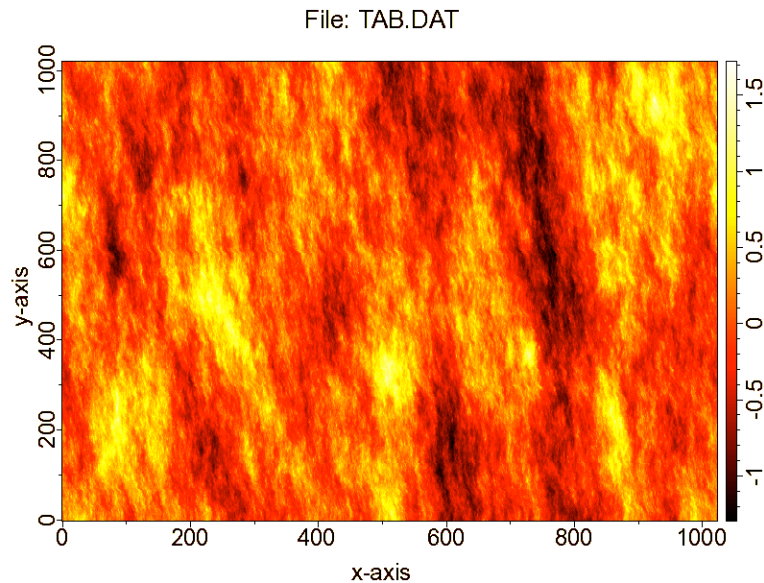


Fig. 7. A simulated instantaneous intensity pattern on the ground calculated assuming a typical low frequency signal with an axial ratio of 5, a minor axis of the ellipse of the order of 100 metres, a $1/f$ noise spectrum and a direction-of-arrival of 60 degrees,

The signal recorded at a microphone may be reproduced from the graph in Fig. 7 by moving the microphone from the initial position ($x=0, y=300$) in the direction of the angle-of-arrival with a speed corresponding to the trace velocity of 300 m/sec. The resulting amplitude and the corresponding wavelet spectrum are shown in Fig. 8.

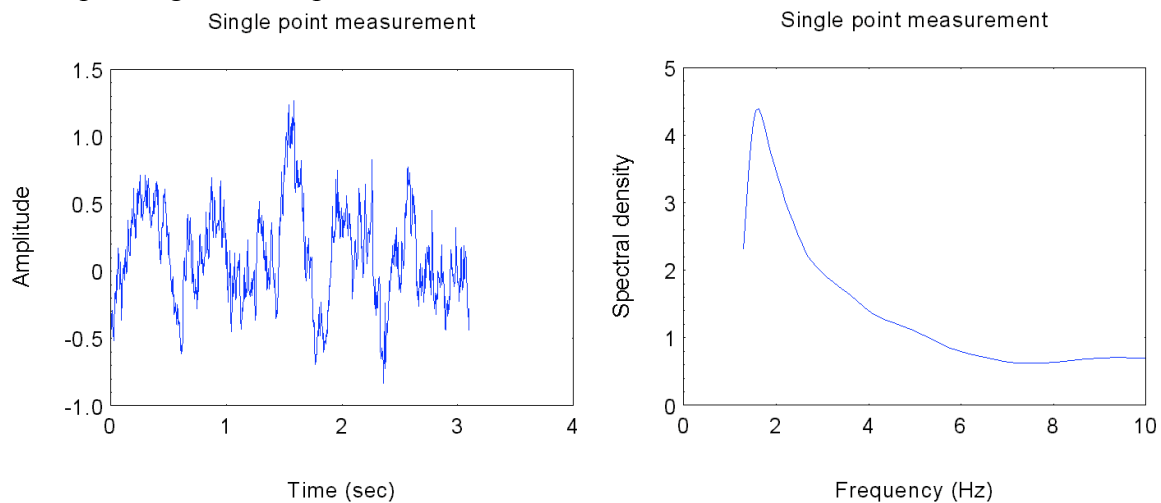


Fig. 8 Amplitude recording from a single point microphone moving across the intensity field in Fig. 7 (left graph) and the corresponding frequency spectrum (right graph).

The present technique offers a method for testing how different spatial filters influence the recorded signal. In this type of device a pressure signal is picked up through inlet ports in a wave-guide, where all contributions are added to a resultant signal. The purpose of the device is to remove stochastic pressure fluctuations and preserve the phase-coherent contributions from the infrasound waves. Four different filters will be simulated here:

1. A straight 101 m pipe (Daniels pipe) with inlet ports at each even metre. When the pipe is:
 - 1a. perpendicular to the direction of propagation, the resulting signal and frequency spectrum are shown in Fig. 9.

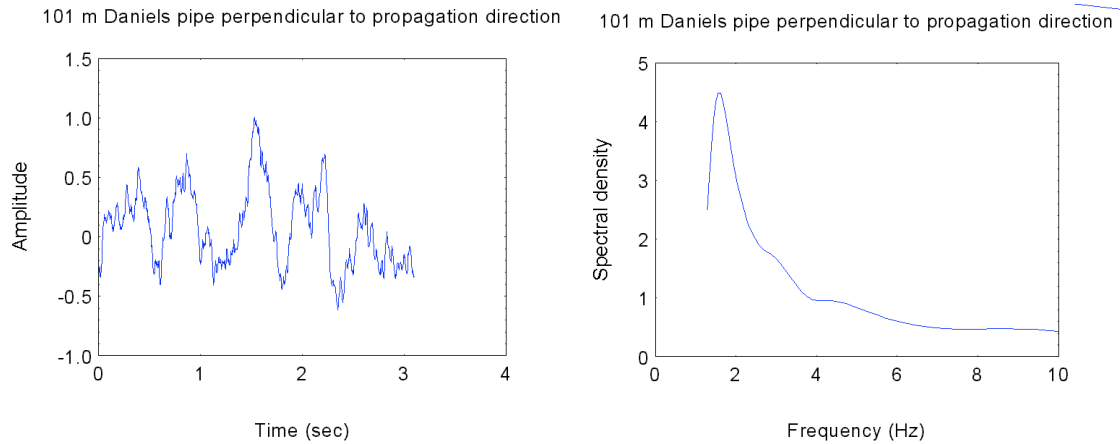


Fig. 9. Amplitude recording from a 101 m Daniels pipe perpendicular to the direction of propagation, moving across the intensity field in Fig. 7 (left graph) and the corresponding frequency spectrum (right graph).

- 1b. parallel to the direction of propagation, the resulting signal and frequency spectrum are shown in Fig. 10.

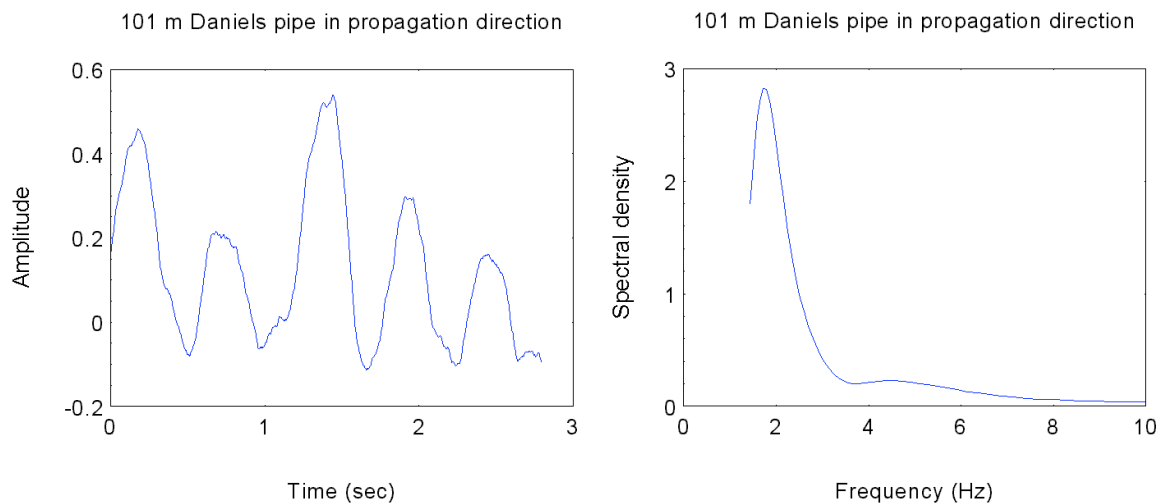


Fig. 10. Amplitude recording from a 101 m Daniels pipe parallel to the direction of propagation, moving across the intensity field in Fig. 7 (left graph) and the corresponding frequency spectrum (right graph).

Observe that the Daniels pipe parallel to the propagation direction acts as a very efficient low-pass filter, but at the expense of the signal amplitude (as compared to the amplitude in Fig. 8.).

- 18-inlet port 20 m circular filter where all signals are collected in a central manifold (Fig. 11)

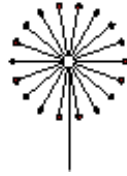


Fig. 11. 18-inlet port 20 m circular filter where all signals are collected in a central manifold

When the circular 18 inlet ports filter moves across the intensity field in Fig. 7, the results shown in Fig 12 are obtained.

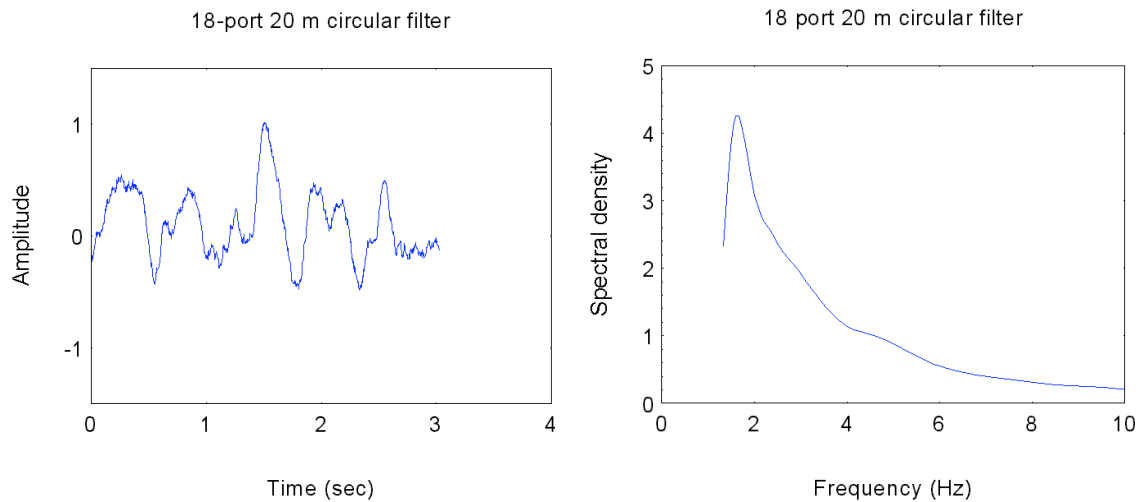


Fig. 12. An amplitude recording from a circular 18 inlet port 20 m filter moving across the intensity field in Fig. 7 (left graph) and the corresponding frequency spectrum (right graph).

- A large, 144 inlet port, spatial filter consisting of 8 filters (Fig 11). The filter is shown in Fig. 13.

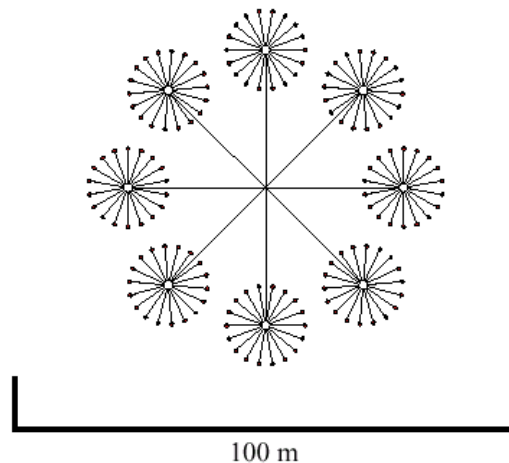


Fig. 13. A large, 144 inlet port, spatial filter consisting of 8 filters (Fig 11) (after Hedlin, 2000).

The signal obtained from this type of filter, when it moves across the intensity field is shown in Fig. 22 together with its frequency spectrum.

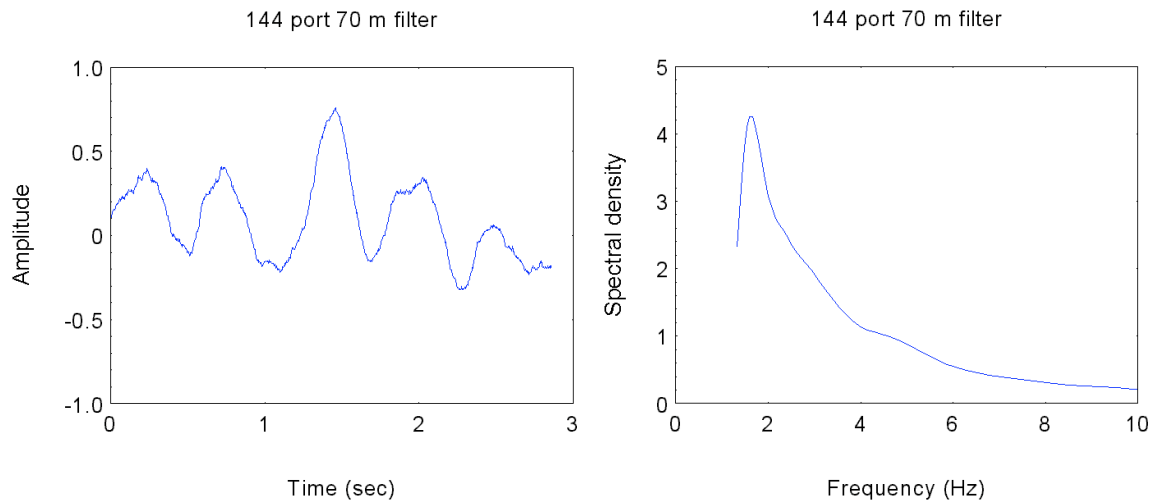


Fig. 14. An amplitude recording from a large 144 inlet port filter moving across the intensity field in Fig. 7 (left graph) and the corresponding frequency spectrum (right graph).

It may be seen that the last filter produces a strong signal and an efficient low-pass filtering. However, the maximum amplitude loss, as compared to the unfiltered signal, is as much as 4.8 dB. That means, that weak signals may be lost during the spatial filtering process.

Signal attenuation in filters has not been taken into consideration in the present simulation.

Since special filters work by averaging the signal across the wave field, the influence on the signal will be different in the direction of propagation than in the direction perpendicular to it. In the direction of propagation there will be an amplitude loss depending on the filter size in this direction. In particular, the filter will totally attenuate the frequency corresponding to a wavelength equal to the filter dimension in the direction of propagation (see Fig. 15). The filter dimension in the direction perpendicular to the direction of propagation is not as critical.

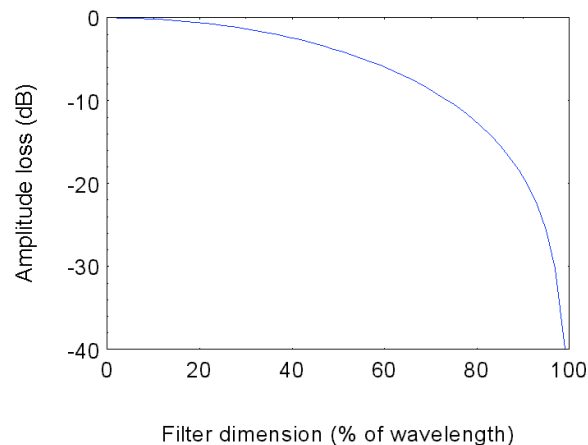


Fig. 15. The amplitude loss depending on the filter dimension in the propagation direction. The filter size is expressed in percent of the wavelength of the recorded signal.

If the filter size in the propagation direction is larger than about 30% of the recorded wavelength, signal attenuation must be taken into account. For broad-band signals the dimension of the filter in the propagation direction will be a factor influencing the rise time of transients.

4. Wind shelters

The wind noise, generated by the turbulence in the airflow, is the major obstacle in detecting of distant infrasonic signals. The dominating wind noise reduction system is based on spatial filtering. In spatial filtering the total sound pressure signal is collected at a large number of low-impedance inlets distributed over a large area (see previous section), and further on by a system of pipes gathering the total signal at a central transducer. It is assumed that the wind noise will be averaged out over the area of the filter, while the infrasonic signal will add-up to its average value across the filter. It is valid under the assumption that the signal coherence above the entire filter is constant. In the opposite case the phase of the averaged signal will be modified in an unpredictable way.

At the Swedish-Finnish Infrasound Network the problem of wind noise was solved using wind barriers (see Fig. 16). The circular wind barrier, used in the SFIN arrays, has been developed and patented by L. Liszka in 1975 (Swedish Patent No. 7315138-3, October 30, 1975).

A wind barrier removes the turbulence from the immediate surroundings of the microphone. The advantage of the wind barrier is that the microphone records the sound pressure at a single point in space, without averaging over a large area. Spatial filters and wind barriers were compared experimentally by Hedlin and Raspert (2003). Results of the investigation are quoted below.

Concerning the wind noise reduction:

“Comparison of the scaled reductions in wind noise produced by the rosettes and wind barrier with the reductions afforded by a spherical wind screen hold promise for significant wind noise reduction with a smaller foot print device. The rosettes only produce reductions if the scale size of the turbulence is smaller than the size of the rosette since such devices rely on the incoherence of the turbulence at each port. The wind barrier displayed large reductions only when the scale size of the turbulence is smaller than the height of the barrier. However, a small reduction of about 4 dB was realized when the scale size was larger than the barrier. This reduction may correspond to the large reductions realized by foam windscreens. In the spherical windscreens, these reductions occur since the pressure measured at the center is the area average of the pressures generated at the surface of the sphere. For large turbules, the pressure generated by an increase in wind speed is positive at the front of the sphere and negative at the back, and the average is less than the pressure measured at a bare sensor. This result holds promise that a properly designed windscreen on or near the ground surface may achieve significant reductions even for turbulence scales greater than the size of the screen.” .

The authors' conclusions concerning preservation of signals while attenuating noise:

“Ultimately, we seek a device that will provide maximum attenuation of unwanted noise and minimally distorted recordings of signals from remote sources. Signals and noise are received at a single point inside the barrier. This is potentially a significant advantage of the barrier over spatial filters, such as the two considered in this paper, which rely on the different coherence lengths of signal and noise. Spatial filters are used to increase the ratio of signal-to-noise by sampling air pressure at numerous locations at offsets at which the noise is believed to be incoherent and the signal remains coherent. If phasing between the multiple samples of the signal is not correctly taken into account, and if the signal is not coherent across the area spanned by the spatial filter, the waveform of the signal will be degraded. Rosette filters are tuned to signals arriving with infinite phase velocity. Signal attenuation caused by 70-meter aperture rosette filters becomes acute at low angles of incidence and at frequencies above 1

Hz (Hedlin, Douze and Herrin, 2002)”.

The final conclusion:

“Unlike spatial filters currently in use at IMS array sites, the barrier does not propagate the signals through narrow pipes. Ambient signal and noise enter the microbarometer from free-air and therefore, dispersion of broad-band signals that is known to occur in narrow pipes (e.g. Benade, 1968) is not a concern”.

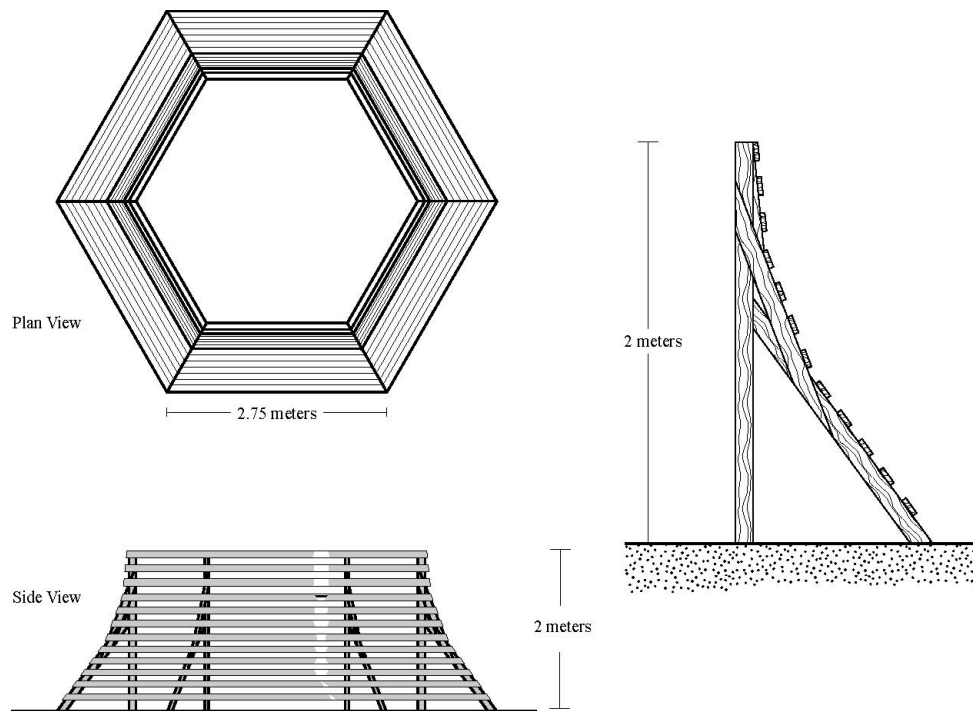


Fig. 16. A wind barrier of the type used at SFIN recording stations

A theory of wind shelters has been developed by ReVelle (2008).

5. The anisometry of the cross-correlation on the ground and the inter-microphone distances in infrasonic arrays

Not all wave packets reaching the array may be detected. As was mentioned in earlier sections the cross-correlation over the array may be described as an ellipse. The minor axis of the ellipse is determined by the dominating frequency of the signal. The major axis is perpendicular to the direction of propagation. The major axis is thus the part of the wave front along which the signal is correlated. The infrasonic waves cannot be visualized as a system of infinite wave fronts. The correlation distances shorter than half of the shortest distance between microphones cannot be measured. It has been found that correlation lengths down to 40 metres may be determined for arrays of the Swedish-Finnish Infrasonic Network with the shortest distance between microphones of 75 metres. In other words the arrays cannot detect small wave packets with correlation distances along the wave fronts shorter than 40 metres.

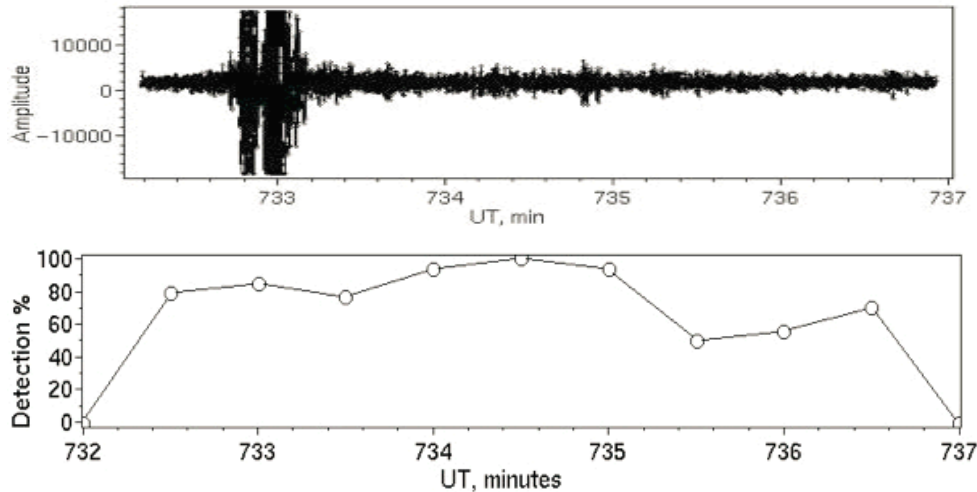


Figure 17. Amplitude recording from Kiruna of the explosion on August 21, 2006 (upper graph), together with the percentage of detection, detectibility (lower graph).

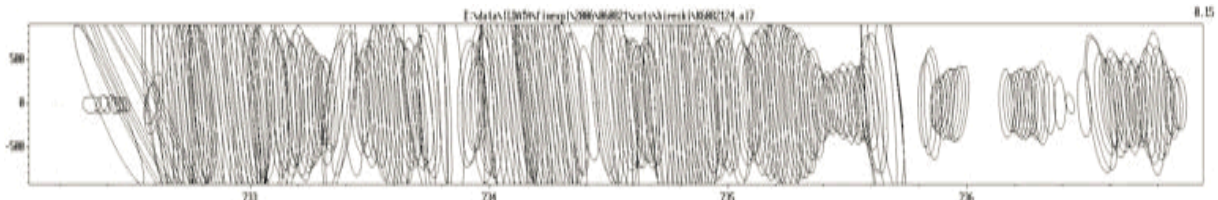


Figure 18. Correlation ellipses for the explosion of August 21, 2006, plotted on the xy-plane, with North directed upwards. The x-axis is also the time axis (in minutes UTC) and the centre of each ellipse is plotted at the respective time of observation. The vertical scale is in metres.

The major axis of the correlation ellipse is thus a measure of the size of an individual wave packet. As an example, the correlation ellipses for the explosion signal shown in Fig. 17 are shown in Fig. 18. The explosion signal arrives from the direction of 85.4° . It is possible to simulate arrays with different distances between the microphones by removing readings for wave packets smaller than a given threshold value, characteristic for a certain smallest distance between microphones.

Fig. 19 presents an example of simulated percentage of detection, or detectibility (Liszka et al. 2008) for the explosion shown in Figs. 17 and 18 and for four different correlation distances. It is apparent that when the minimum distance between the microphones exceeds 500 meters, the detectibility drops dramatically and the coherent signal extracted from two microphones starts to show several separate “arrivals”.

An interesting conclusion may be drawn studying variations of the major axis of the ellipse as a function of time (Fig. 18). A number of very large values of the major axis are embedded in a continuum of much smaller values. An inspection of the distribution of the recorded values on the major axis indicates that the distribution is not uniform and that there is an excess of very large values (>1000 metres). This property of the distribution may be a reason why short bursts of the signal from weak sources may, sometimes, be detected at considerable distances. It is usually assumed that large distances between microphones in an array guarantee the array’s performance. It may be true under the assumption that distances between its microphones are kept short (preferably under 100 metres). No matter which detection principle is used, the large distances between microphones mean that different wave packets, often travelling along different propagation paths, are treated as parts of the same wave front.

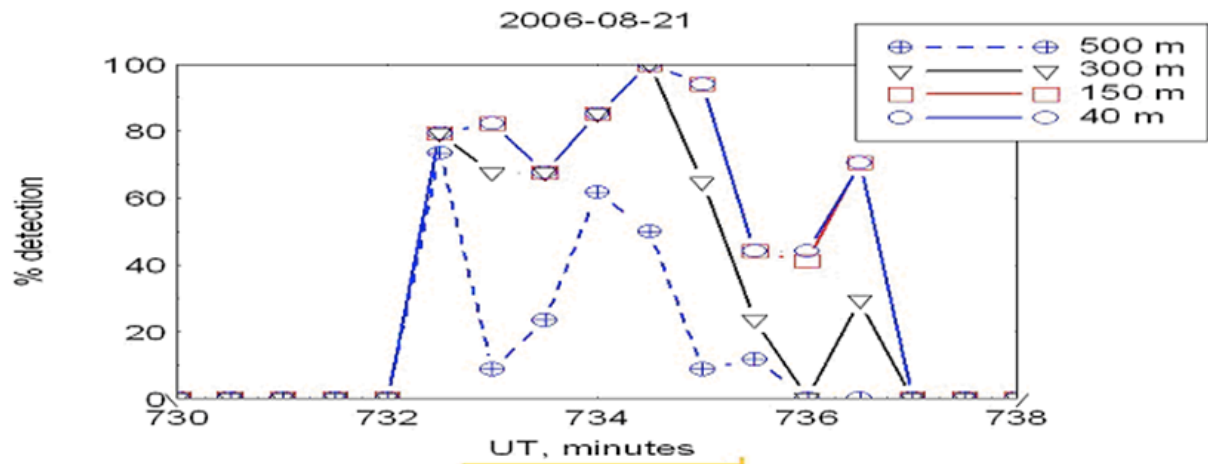


Figure 19. Detectibility for the explosion signal recorded in Kiruna on August 21, 2006, for different minimum distances between microphones.

Conclusions

The parameters of the correlation ellipse on the ground seem to be related to the spectral content of the signal (the minor axis) and thus to the nature of the source. Since, during the long distance propagation, the atmospheric irregularities will influence the statistical properties of the signal, the properties of the correlation ellipse will also be related to the distance to the source and to the actual atmospheric structure.

The statistical properties of the signal provide important information necessary for appropriate design of the detecting systems. In particular, it appears that the use of spatial filters introduces serious distortion and attenuation of observed signals. The main conclusion is therefore that the wind noise should be removed using wind shelters and not spatial filters/pipe arrays.

Increasing the distance between microphones within an array does not increase the detectibility of infrasonic signals, although it does increase the accuracy of the determined angle-of-arrival. The selection of distance between microphones must be a compromise between the accuracy of the angle-of-arrival and the probability of detection.

References

- Davies, K., 1972: Some analogies between propagation of ionospheric radio waves and acoustic gravity waves. In *Effects of Atmospheric Acoustic Gravity Waves on Electromagnetic Wave Propagation*, AGARD Conference Proceedings No 115.
- Hedlin, M. A., and R. Raspet, 2003: Infrasonic wind-noise reduction by barriers and spatial filters. *J. Acoust. Soc. Am.* 114 (3): 1379-86.
- Koster, J. R., I. Katsriku, and M. Tete, 1965: *Studies of the Equatorial Ionosphere Using Transmissions from Active Satellites*. Annual Summary Report No. 1. Contract No. AF61(052)-800. Dept. of Physics, University of Ghana – Legon, Accra, Ghana.
- Liszka, L., 1963: *Auroral zone ionosphere investigations using transmissions from artificial earth satellites*. Doctoral thesis. Uppsala: Almqvist & Wiksell.
- Liszka, L., 1974: Long-distance propagation of infrasound from artificial sources. *J. Acoust. Soc. Am.*, 56 (5): 1383-1388.
- Liszka, L., C. Enell and T. Raita, 2009: Infrasound in the Atmosphere - towards a new propagation model, *Inframatics*, June 2009, 1-14
- ReVelle, D., 2008, “Infrasonic Noise Reduction Using Shelters/Windbreaks”. Paper presented at Infrasound Technology Workshop, Bermuda, November 2008.



Institutet för rymdfysik

Swedish Institute of Space Physics

Swedish Institute of Space Physics
Box 812, SE- 981 28 Kiruna, SWEDEN
tel. +46-980-790 00, fax +46-980-790 50, e-post: irf@irf.se

www.irf.se